Magnetocaloric effects, quantum critical points, and the Berezinsky-Kosterlitz-Thouless transition in two-dimensional coupled spin-dimer systems

Dominik Straßel,[1,*] Peter Kopietz,[2] and Sebastian Eggert[1]

[1]*Department of Physics and Research Center Optimas, Technical University Kaiserslautern, 67663 Kaiserslautern, Germany*

[2]*Department of Theoretical Physics, Goethe-University Frankfurt, 60438 Frankfurt, Germany*

(Received 5 February 2015; revised manuscript received 19 March 2015; published 6 April 2015)

Spin-dimer systems are a versatile playground for the detailed study of quantum phase transitions. Using the magnetic field as the tuning parameter, it is possible to observe a crossover from the characteristic scaling near critical points to the behavior of a finite-temperature phase transition. In this work we study two-dimensional coupled spin-dimer systems by comparing numerical quantum Monte Carlo simulations with analytical calculations of the susceptibility, the magnetocaloric effect, and the helicity modulus. The magnetocaloric behavior of the magnetization with temperature can be used to determine the critical fields with high accuracy, but the critical scaling does not show the expected logarithmic corrections. The zeros of the cooling rate are an excellent indicator of the competition between quantum criticality and vortex physics, but they are not directly associated with the quantum phase transition or the finite-temperature Berezinsky-Kosterlitz-Thouless transition. The results give a unified picture of the full quantum and finite-temperature phase diagram.

DOI: 10.1103/PhysRevB.91.134406 PACS number(s): 75.10.Jm, 75.30.Sg, 75.30.Kz, 05.30.Jp

I. INTRODUCTION

The study of quantum phase transitions (QPTs) remains a very active topic in many fields of physics, spurred by experimental progress in creating novel tunable interacting systems. QPTs occur in quite different materials, including heavy fermion compounds, unconventional superconductors, Mott insulators, coupled spin systems, and ultracold atoms. In particular, the common phenomenon of Bose-Einstein condensation (BEC) of strongly interacting bosons by tuning the interaction or the chemical potential can now be found in a range of different physical systems. Ultracold atomic gases allow the tuning of interactions via Feshbach resonances, but also cross-dimensional phase transitions [1] and Berezinsky-Kosterlitz-Thouless (BKT) behavior [2] have been observed recently. Phase transitions in coupled spin-dimer systems are prime examples of BEC of strongly interacting triplons [3–8], which allow easy tuning of the chemical potential via the magnetic field. Although QPTs occur at zero temperature as a function of a nonthermal control parameter such as the interaction, effective mass, or the chemical potential, a characteristic critical scaling with temperature can be observed in a large range above the critical point [4]. In general a detailed analysis is necessary in order to understand how the critical behavior is reflected in the experiments and if the finite-temperature phase transition is affected in the vicinity the QPT, where thermal fluctuations are comparable to quantum fluctuations. Compared to bosonic gases of atoms and magnons, temperature control is relatively easy in triplon gases, which allows a systematic analysis of the critical scaling behavior near the QPT.

In this paper we focus on the theoretical analysis of quantum critical points of antiferromagnetic spin-dimer systems which are weakly coupled in two dimensions. Two QPTs can be observed: As the field is increased through the lower critical value B_c the spin dimers start to be occupied by triplons and the magnetization increases with characteristic two-dimensional logarithmic behavior. The second QPT corresponds to the saturation field B_s. The intermediate phase is characterized by long-range phase coherence of triplons at $T = 0$ and BKT behavior [9–12] at finite T. Similar phase transitions occur in two-dimensional hard-core boson systems[13] and in distorted frustrated lattices [14].

The schematic behavior is illustrated in Fig. 1. In this paper we show that the crossover from BKT behavior to critical scaling is rather well defined by the cooling rate and by characteristic maxima in the susceptibility. However, this crossover occurs at distinctly higher temperatures than the BKT transition which can be determined by a careful analysis of the spin stiffness. There is no directly measurable signal for the BKT transition in experiments [3], but we find that magnetocaloric measurements are ideally suited to show the critical scaling and to pinpoint the exact location of the QPT. Close to the QPT the BKT transition retains the characteristic logarithmic behavior, albeit with strongly renormalized parameters. We find, however, that the low-temperature behavior above the QPTs does not fully follow theoretical expectations.

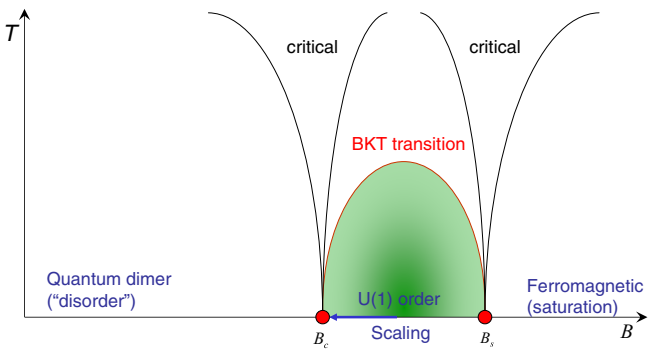

FIG. 1. (Color online) Schematic phase diagram of the coupled spin-dimer model with Hamiltonian given in Eq. (1).

*strassel@physik.uni-kl.de

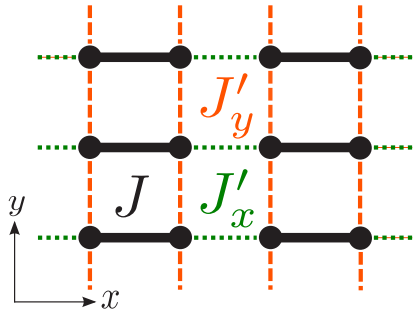

FIG. 2. (Color online) Coupled dimers on a square lattice, with a columnar arrangement of the dimers.

II. MODEL

We use a "columnar" arrangement of strongly coupled antiferromagnetic dimers ($J > 0$) on a two-dimensional square lattice as shown in Fig. 2, described by the Hamiltonian of localized spin-1/2 operators $\hat{\vec{S}}_{x,y}$

$$H = \sum_{y=1}^{N_y} \Bigg[\sum_{x=\text{odd}}^{N_x} J \hat{\vec{S}}_{x,y} \cdot \hat{\vec{S}}_{x+1,y} + J'_x \hat{\vec{S}}_{x+1,y} \cdot \hat{\vec{S}}_{x+2,y} + J'_y \sum_{x=1}^{N_x} \hat{\vec{S}}_{x,y} \cdot \hat{\vec{S}}_{x,y+1} \Bigg] - B \sum_{i=1}^{N} \hat{S}^z_i, \tag{1}$$

where the interdimer couplings J'_x and J'_y can be ferromagnetic or antiferromagnetic, but are assumed to be small $|J'| \ll J$.

A. Interacting boson models

Assuming that the intradimer exchange interaction J dominates over interdimer couplings J'_x and J'_y, it is natural to represent the system in the singlet and triplet basis at each dimer site

$$\begin{aligned} |\,t_-\,\rangle_i &= |\downarrow\downarrow\rangle_i, \quad |\,t_0\,\rangle_i = \frac{|\uparrow\downarrow\rangle_i + |\downarrow\uparrow\rangle_i}{\sqrt{2}}, \\ |\,t_+\,\rangle_i &= |\uparrow\uparrow\rangle_i, \quad |\,s\,\rangle_i = \frac{|\uparrow\downarrow\rangle_i - |\downarrow\uparrow\rangle_i}{\sqrt{2}}. \end{aligned} \tag{2}$$

At strong fields $B \approx J$ the last two states become nearly degenerate, while the other two higher energy states will be neglected for now. It is therefore justified to work in a restricted Hilbert space with only two states at each dimer site, which are represented by hard-core bosons on the vacuum $|0\rangle = \prod_i |\,s\,\rangle_i$ and $b_j^\dagger |0\rangle = |\,t_+\,\rangle_j \prod_{i\neq j} |\,s\,\rangle_i$. In this Hilbert space the effective Hamiltonian describes strongly interacting bosons on a rectangular lattice

$$H_{\text{eff}} = \sum_{\langle i,j\rangle} [-|t_{ij}|(b_i^\dagger b_j + b_j^\dagger b_i) + t_{ij} n_i n_j] - \mu \sum_i n_i + U \sum_i n_i(n_i - 1), \tag{3}$$

where the limit $U \to \infty$ is implied to satisfy the hard-core constraint. The effective chemical potential and the hopping in x and y directions are given by

$$\mu = B - J, \quad t_x = J'_x/4, \quad t_y = J'_y/2. \tag{4}$$

Note that the hopping $|t_{ij}|$ in Eq. (3) has been chosen to be positive, which can always be achieved by a local gauge transformation $b_i \to (-1)^i b_i$. The nearest neighbor interaction in Eq. (3) is repulsive (attractive) for $J' > 0$ ($J' < 0$). By Fourier transforming the first term in the Hamiltonian the kinetic energy becomes

$$H_{\text{kin}} = \sum_{\vec{k}} (-2|t_x| \cos k_x - 2|t_y| \cos k_y) b_{\vec{k}}^\dagger b_{\vec{k}}. \tag{5}$$

The position of the upper and lower band edges allows a straight-forward estimate of the critical fields B_c and B_s. The lower critical field is determined by the chemical potential at which a single boson acquires positive energy $-2|t_x| - 2|t_y| = \mu$, which gives

$$B_c \approx J - |J'_x|/2 - |J'_y|. \tag{6}$$

This estimate is only correct to first order in J', however, because the bosonic ground state (vacuum) is not an exact eigenstate of the full Hamiltonian in Eq. (1). Higher order corrections from the neglected triplet states $|\,t_-\,\rangle$ and $|\,t_0\,\rangle$ in Eq. (2) will be determined from numerical simulations as described below.

The upper critical field is determined from the energy gain of removing a particle from the fully occupied band including the nearest neighbor interaction energy

$$B_s = J + |J'_x|/2 + |J'_y| + J'_x/2 + J'_y, \tag{7}$$

which is exact and corresponds to the saturation field of the original model (1). For intermediate fields $B_c < B < B_s$ the physics is governed by the behavior of two-dimensional interacting bosons (BKT phase) as explained below.

B. Effective continuum model

We now focus on the lower QPT at B_c which corresponds to the well-studied case of a dilute interacting Bose gas [15]. The lattice model in Eq. (3) is believed to show a quantum phase transition to a long-range XY-ordered phase at $T = 0$ when the chemical potential is increased above a critical value. In the continuum limit the nearest neighbor interaction can be neglected and the hard-core constraint can be replaced by a strong ϕ^4 interaction of a complex bosonic field $\phi(\vec{r},\tau)$ in a $(D+1)$-dimensional Euclidean action

$$S = \int_0^\beta d\tau \int d^D r \left[\bar{\phi} \left(\partial_\tau - \frac{\vec{\nabla}^2}{2m} - \tilde{\mu} \right) \phi + \frac{u_0}{2} |\phi|^4 \right], \tag{8}$$

where $D = 2$ in our case. The parameters can be obtained by approximating the sums in Eq. (3) by integrals and then rescaling $x' = x(t_y/t_x)^{1/4}$ and $y' = y(t_x/t_y)^{1/4}$. The resulting estimates

$$m = \frac{1}{2a^2\sqrt{|t_x t_y|}}, \quad \tilde{\mu} = B - B_c, \quad u_0 = U a^2, \tag{9}$$

are only approximate, since the renormalization from eliminating the large-wave-vector modes in Eq. (8) has been neglected. In what follows we set the lattice spacing to unity $a = 1$.

The action in Eq. (8) describes an interacting dilute Bose gas with mass m and chemical potential $\tilde{\mu}$. For $\tilde{\mu} > 0$ or $B > B_c$ a finite density of bosons appears even at zero temperature

$T = 0$, which signals the QPT to the BKT phase. Analogously, the same model also applies at the upper critical field B_s, where it describes bosonic singlet excitations on the saturated state with $\tilde{\mu} = B_s - B$.

The upper critical dimensions is $D = 2$ for this model so that logarithmic corrections appear in this case, which are described in terms of an ultraviolet cutoff Λ_0 (of the order of the reciprocal rescaled lattice spacing). This situation ($D = 2$) has been analyzed extensively in the literature [16–23] for various quantities which we summarize below. Other dimensions are discussed in the textbook of Sachdev [15].

The density of bosons corresponds to the magnetization per site $\langle \bar{\phi}\phi \rangle = 2M(B)/N$ in the spin-dimer system as a function of field $\tilde{\mu} = B - B_c$, which is given at $T = 0$ by [16]

$$\frac{M}{N} = \frac{m\tilde{\mu}\,\Theta(\tilde{\mu})}{8\pi} \ln\left[\frac{\Lambda_0^2}{2m\tilde{\mu}}\right]. \tag{10}$$

The susceptibility is therefore

$$\chi = \frac{m}{8\pi}\left(\ln\left[\frac{\Lambda_0^2}{2m\tilde{\mu}}\right] - 1\right), \tag{11}$$

which is logarithmically divergent as the critical point is approached from above inside the BKT phase $B \to B_c$. For $T > 0$ and $B = B_c$ it has been predicted that the density increases with temperature including a characteristic logarithmic correction [16]

$$M(T) = \frac{mT}{4\pi} \ln^{-4}\left[\frac{\Lambda_0^2}{2mT}\right]. \tag{12}$$

The scaling as a function of T can be used to identify the exact value of the critical field B_c as outlined below.

Finally, the BKT transition temperature has been predicted as a function of field [18]

$$T_{\mathrm{BKT}} = \frac{\tilde{\mu}}{4} \frac{\ln\left[\frac{\Lambda_0^2}{2m\tilde{\mu}}\right]}{\ln\left(\ln\left[\frac{\Lambda_0^2}{2m\tilde{\mu}}\right]\right)}. \tag{13}$$

However, for this formula to be valid the double logarithm has to become very large, which does not correspond to physically relevant regions [18,19]. In fact, it remains to be seen if the single logarithms in Eqs. (10)–(12) are large enough so that the leading behavior can be observed in our numerical simulations below and in future experiments.

III. DETERMINING THE CRITICAL FIELDS

To analyze the quantum phase transitions, the exact locations of the critical fields have to be determined first. As mentioned above, the upper critical field B_s is exactly the saturation field in Eq. (7), but the lower field in Eq. (6) will in general have higher order corrections of the form

$$B_c \approx J - |J_x'|/2 - |J_y'| + a_x J_x'^2 + a_y J_y'^2 + a_{xy} J_x' J_y'. \tag{14}$$

The higher order corrections are due to virtual excitations to the neglected triplet states $|t_-\rangle$ and $|t_0\rangle$ in Eq. (2). The exact values for $a_x = -0.375$ and $a_y = 0.5 J_y$ are known from higher order strong coupling expansions for the dimerized chain [24,25] ($J_y' = 0$) and for the ladder system [26] ($J_x' = 0$), respectively.

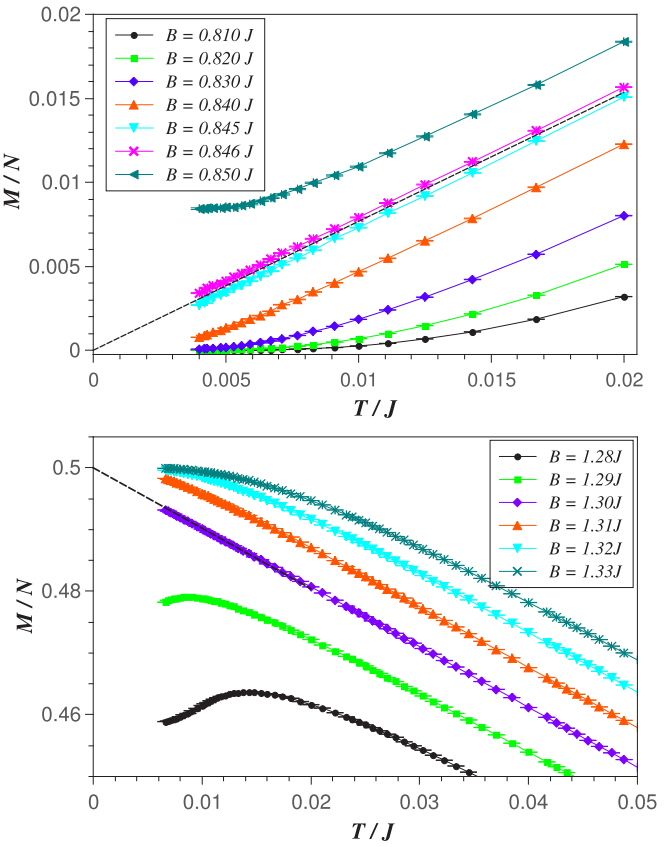

FIG. 3. (Color online) QMC data for the magnetization as a function of temperature for different magnetic fields for $J_x' = J_y' = 0.1$ and $N = 676$ near B_c (top) and B_s (bottom). The lines are linear fits at the critical fields.

To determine the exact location of the QPT for general interdimer couplings, numerical simulations at $T = 0$ in the thermodynamic limit would be required. This is obviously impossible, but large system sizes at small finite temperatures are feasible with quantum Monte Carlo (QMC) simulations. To examine the model in Eq. (1) numerically, we therefore have implemented the stochastic series expansion algorithm [27] with directed loop updates and using the so-called Mersenne Twister random number generator [28].

At finite temperatures the discontinuity in the first derivative of Eq. (10) cannot be observed directly, but the magnetization as a function of temperature becomes exponentially small for $B < B_c$ while it approaches a finite value for $B > B_c$. The critical field B_c is then exactly defined as the point where critical scaling is obeyed, which can be determined rather accurately. This behavior is illustrated in Fig. 3.

Note, however, that the observed scaling in Fig. 3 at the exactly known upper critical field B_s appears to be perfectly linear (relative to the saturated state). This means that the logarithmic correction in Eq. (12) must be very small, which puts a lower limit on the cutoff $\Lambda_0 \gtrsim 10^7$. To determine the lower critical field B_c, we therefore use linear scaling as well. Extrapolating the data to the thermodynamic limit and then determining the critical fields B_c by the best linear fit gives the results for three different choices of interdimer couplings shown in Table I. Ignoring higher orders, the values for the

TABLE I. Critical field B_c for three different choices of exchange couplings, which obey the condition $J_x' + 2J_y' = 0.3J$, i.e., $B_c \approx 0.85J$ to lowest order.

Case	t_x/J	t_y/J	B_c/J ± 0.0005	From Eqs. (14), (15)
$J_x' = J_y' = 0.1J$	0.025	0.05	0.8460	0.84625
$J_x' = 2J_y' = 0.15J$	0.0375	0.0375	0.8391	0.83875
$2J_x' = J_y' = 0.12J$	0.015	0.06	0.8523	0.85225

coefficients in Eq. (14) are then consistent with the following estimates:

$$a_x = -0.375, \quad a_y = 0.5, \quad a_{xy} \approx -0.5 \pm 0.03. \qquad (15)$$

Before continuing our analysis we would also like to consider how the neglected higher energy triplet excitations $|t_-\rangle$ and $|t_0\rangle$ in Eq. (2) affect physical observables like the magnetization. We note that the effective Hamiltonian (3) is invariant under changing interdimer coupling strengths J_x' and J_y' as long as all energies and the field μ are rescaled accordingly. We therefore consider three different realizations of the coupling strength $J_x' = J_y' = J' = 0.05J$, $0.1J$, and $0.2J$ and plot the susceptibility $\chi J'$ as a function of rescaled field $\mu/J' = (B - J)/J'$ at a given rescaled temperature $\beta J' = 5$ in Fig. 4. We observe a finite susceptibility in the BKT phase with two characteristic maxima near the QPT. While the three curves agree reasonably well, systematic deviations can be seen for larger J', which can only come as a result of corrections from the higher energy triplet excitations. In what follows we choose the coupling strengths $J_x' = J_y' = J' = 0.1J$, which is a compromise between minimizing higher order corrections and efficient numerical simulations. It is believed that the higher order triplet excitations do not change the form of the critical scaling in Eqs. (10)–(13).

IV. CRITICAL SCALING AT THE QPT

We now turn to analyzing the scaling behavior of the susceptibility χ as a function of field B in Eq. (11). Finite

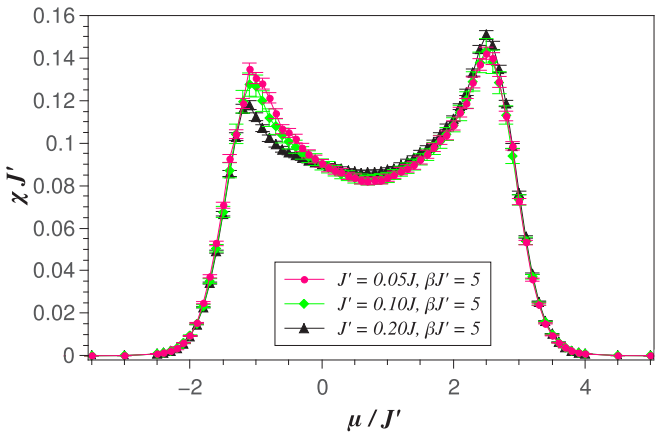

FIG. 4. (Color online) QMC data for the susceptibility $\chi J'$ as a function of $\mu/J' = (B - J)/J'$ at inverse temperature $\beta J' = 5$ for three interdimer coupling strengths $J_x' = J_y' = J' = 0.05J, 0.1J$, and $0.2J$.

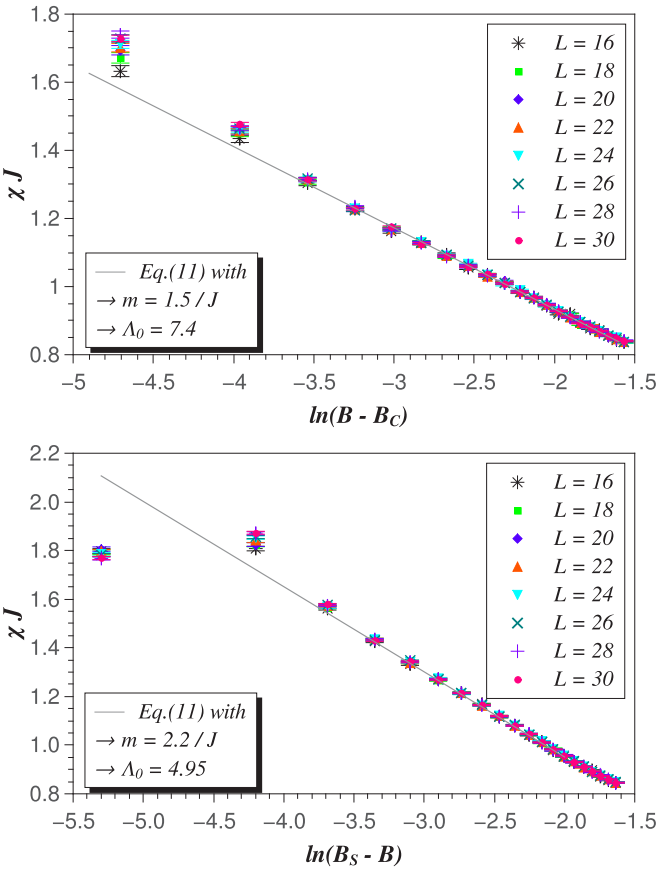

FIG. 5. (Color online) QMC data of the susceptibility for different system sizes $N = L \times L$ and an inverse temperature of $\beta J = 200$ for $J_x' = J_y' = J' = 0.1J$ near B_c (top) and B_s (bottom). The lines represent the best fit to the prediction in Eq. (11).

temperatures T and system sizes $N = L \times L$ play the role of an infrared cutoff $D_0 \sim \max(T, J'/L)$ which will give deviations from the predicted $T = 0$ scaling in Eqs. (10) and (11) as the QPT is approached. However, for fields $|B - B_{c/s}| \gtrsim D_0$ the scaling can still be tested. At each given temperature we first increase the system size until systematic convergence of the magnetization is obtained as shown in Fig. 5. The resulting susceptibility in the thermodynamic limit near the QPTs is shown in Fig. 6 as a function of the logarithm of $\tilde{\mu} = |B - B_{c/s}|$ for different temperatures.

The data confirms that the scaling approaches a logarithmic behavior for $T \to 0$ consistent with the form in Eq. (11). We notice that the finite-temperature susceptibility is actually rather small at the QPT $B = B_c$, but then increases and *overshoots* the logarithmic divergence before the logarithmic behavior is reached inside the BKT phase. In this way the field integral of the susceptibility (i.e., the magnetization) remains largely temperature independent outside the critical region, since the smaller values at the QPT for finite T are compensated for by a corresponding overshooting of the maximum. In turn this means that the characteristic maxima in Fig. 4 of the susceptibility are only indirectly related to the QPT. The overshooting implies that the large fluctuations in the magnetization arise from a different mechanism at finite temperatures. One may expect that the maxima are therefore

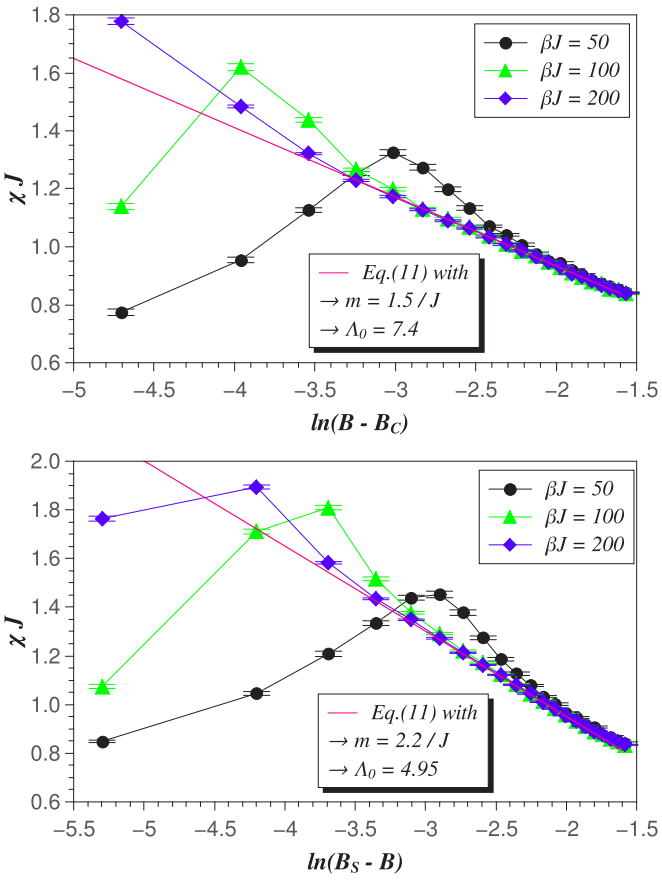

FIG. 6. (Color online) Susceptibility extrapolated to the thermodynamic limit for different inverse temperatures βJ and $J'_x = J'_y = J' = 0.1J$ near B_c (top) and B_s (bottom). The lines represent the best fit to the prediction in Eq. (11).

related to the finite-temperature BKT transition, but this is *not* the case as we will see below. Instead we find that the susceptibility maxima are found for temperatures well above the BKT transition $T > T_{\mathrm{BKT}}$ at the corresponding fields. As we will see later the maxima coincide with maxima in the entropy, so that these points correspond to the crossover between quantum critical scaling to vortex physics.

Comparing with the expected form in Eq. (11) quantitatively, we find rather small values of the effective mass $m \approx 1.5/J$ at the lower QPT B_c and $m \approx 2.2/J$ at B_s, which are strongly renormalized compared to the naive estimate $m \approx 14/J$ according to Eq. (9). The value of $\Lambda_0 \sim 5-7$ remains finite in Eq. (11). The value of m from the fits at the lower QPT is rather sensitive to the exact location of the critical field B_c. In general all microscopic details such as the neglected next-nearest neighbor interaction in Eq. (3) will influence the exact value of the effective parameters in Eq. (9).

V. BEREZINSKY-KOSTERLITZ-THOULESS PHASE TRANSITION

The intermediate region between the two QPTs is dominated by the presence of interacting triplon excitations which form a condensate at $T = 0$ with long-range phase coherence. We now consider the finite-temperature behavior in this intermediate phase. While the QPTs are driven by quantum fluctuations, the transition due to thermal fluctuation corresponds to classical behavior and is therefore not directly related to the scaling discussed above.

The effective hard-core boson model in Eq. (3) is exactly equivalent to the XXZ-spin model with $J_z = J_{xy}/2$, which is known to be in the XY-universality class. At finite temperatures this system undergoes a BKT transition, which can be described in terms of classical two-dimensional spins as first explained in the works of Berezinsky [9,10] and Kosterlitz and Thouless [11,12]. At low temperatures $T < T_{\mathrm{BKT}}$ a quasi-long-range ordered phase with power-law decay of correlations exists. Above the phase transition temperature T_{BKT} the unbinding of vortices is energetically allowed leading to a disordered phase with exponential decaying correlations. Kosterlitz used the spin stiffness [12]

$$\rho_S = \frac{1}{N}\left(\frac{\partial^2 F}{\partial \phi^2}\right)\Big|_{\phi=0} \tag{16}$$

to identify a phase transition, where F is the free energy of the system and ϕ is the angle between spins at opposite edges of the system. To determine the spin stiffness in QMC simulations it is convenient to calculate the winding number fluctuations in each direction [29,30]. This defines the so-called helicity modulus [31] $\gamma = T\langle w^2\rangle = \hbar^2\rho_s/m^2$, which is exactly related to the spin stiffness, where the winding number fluctuation and the change of the angle ϕ are assumed to be in the same direction. The phase transition temperature T_{BKT} involves a slightly different definition of the spin stiffness which may deviate from ρ_s in Eq. (16) for anisotropic systems in low dimensions D as discussed by Prokof'ev and Svistunov [32]. To estimate T_{BKT} in anisotropic systems it is useful to define a rescaled helicity modulus in each direction

$$\begin{aligned}\gamma_x &= T\frac{L_x}{2t_x}\frac{t_y}{L_y}\left\langle\omega_x^2\right\rangle,\\ \gamma_y &= T\frac{L_y}{t_y}\frac{2t_x}{L_x}\left\langle\omega_y^2\right\rangle,\end{aligned} \tag{17}$$

where $L_x/2$ and L_y are the edge lengths of the effective hard-core boson system in terms of the size of the original spin system $N = L_x \times L_y$. Instead of taking the average of γ_x and γ_y, only the largest one $\max(\gamma_x,\gamma_y) = \gamma_x$ is used to estimate T_{BKT}, while the smaller one shows a linear behavior with edge length $\gamma_y \propto L_y$ [32,33].

The phase-transition temperature T_{BKT} is then determined by the value where the largest rescaled helicity modulus obeys in the thermodynamic limit[12]

$$\gamma_x(T_{\mathrm{BKT}}) = \frac{2}{\pi}T_{\mathrm{BKT}}. \tag{18}$$

The energy of the vortices also depend logarithmically on the system size N, so that the condition in Eq. (18) acquires a corresponding correction for finite-size systems [34]

$$\frac{\pi\gamma_x(N,N_0)}{2T} = A(T)\left(1+\frac{1}{2}\frac{1}{\ln(N/N_0)}\right), \tag{19}$$

where N_0 is a fitting parameter and $A(T)$ should take on the universal value of unity at the transition, but can also be used as a fitting parameter [35,36]. Following the procedure in

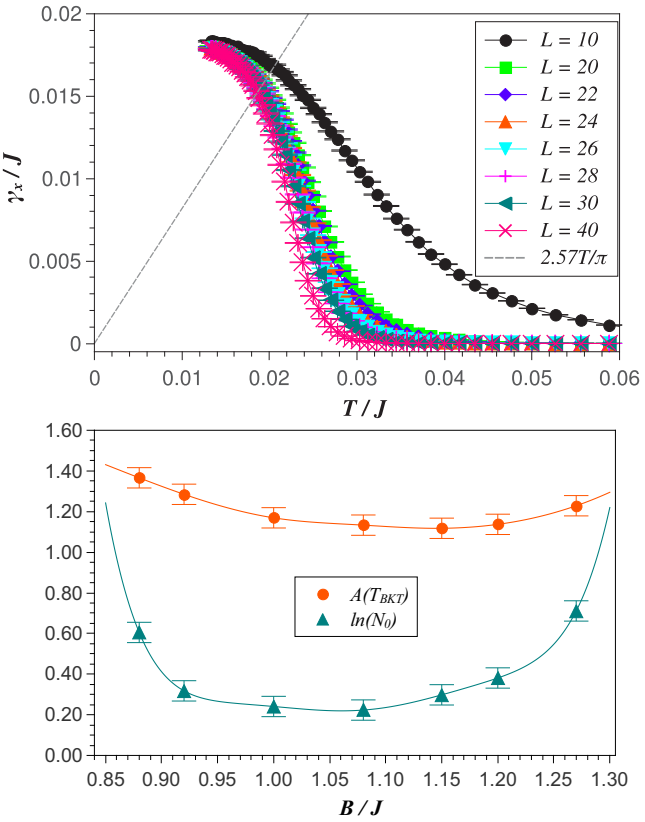

FIG. 7. (Color online) Top: QMC results of the helicity modulus γ_x for different system sizes as a function of temperature at $B = 0.92J$. The finite-size extrapolated intercept with $\gamma_x = 2AT/\pi$ (solid line) determines the BKT temperature. Bottom: $A(T_{\rm BKT})$ and $\ln(N_0)$ as a function of field with the corresponding spline extrapolations (solid lines).

Ref. [35] the logarithmic corrections in Eq. (19) become only accurate at the phase transition, which can in fact be used to determine $T_{\rm BKT}$ and $A(T_{\rm BKT})$. In Fig. 7 the helicity modulus is plotted at a given field $B = 0.92J$ for different system sizes. The BKT transition for each field is determined by the best fit of Eq. (19), i.e., when $\pi\gamma_x(N, N_0)/2T$ extrapolates to a limiting value linearly as a function of $\ln^{-1}(N/N_0)$. For a classical isotropic spin model, a value of $A(T_{\rm BKT}) = 1$ can be confirmed [35,37]; but for the spin-dimer model we find a field-dependent value for $A(T_{\rm BKT})$ which is slightly larger than unity as given in Table II and shown in Fig. 7. The fitting parameter N_0 also becomes field dependent. The resulting transition temperature

TABLE II. Results of $A(T_{\rm BKT})$ and $\ln(N_0)$ for different magnetic fields.

B/J	$A(T_{\rm BKT}) \pm 0.03$	$\ln(N_0) \pm 0.05$	$T_{\rm BKT}/J \pm 0.0005$
0.880	1.37	0.61	0.0103
0.920	1.29	0.32	0.0174
1.000	1.17	0.24	0.0239
1.080	1.14	0.22	0.0245
1.150	1.12	0.30	0.0229
1.200	1.14	0.38	0.0197
1.270	1.23	0.71	0.0092

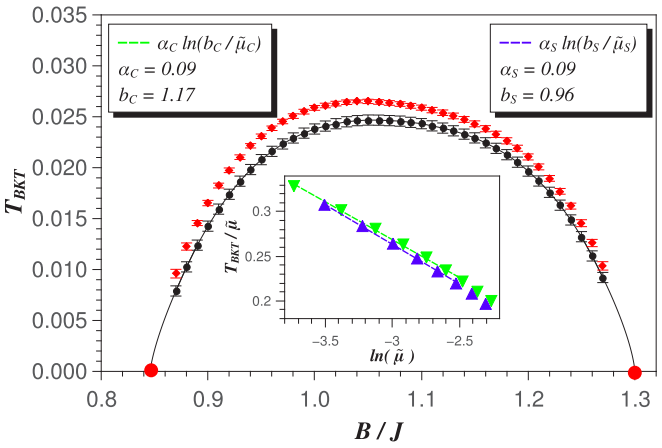

FIG. 8. (Color online) BKT temperature as a function of field using the fitting parameters in Fig. 7 (bottom). The lines connect the data points (black circles) and interpolate the data according to the logarithmic fit in the inset to the critical fields (large red circles). For comparison the results from using fits with a constant value of $A(T_{\rm BKT}) = 1$ are also shown (red diamonds). Inset: Logarithmic behavior according to Eq. (20) (solid lines) near the critical fields.

is shown in Fig. 8, which shows a sharp drop near the QPT. As shown in the inset the behavior is consistent with a logarithmic behavior

$$\frac{T_{\rm BKT}}{\tilde{\mu}} \approx \alpha \ln(b/\tilde{\mu}), \tag{20}$$

but the double logarithmic correction in the asymptotic scaling at extremely small densities in Eq. (13) cannot be confirmed numerically [13].

The deviations from $A(T_{\rm BKT}) = 1$ can be traced to two different sources: In the middle of the BKT phase we find that a nearly isotropic effective system with $L_x = 2L_y$ and $J_x' = 2J_y'$ gives values of $A(T_{\rm BKT}) \approx 1.04$, so that the detailed geometry appears to have some effect on the exact value of A. A second source may be higher order corrections in $\ln N/N_0$, which can be expected to become significant when the effective density of bosons per lattice site is small, which in turn leads to large distances between vortices. Therefore, the corrections must be largest close to the QPT, consistent with our findings. Using a constant value of $A(T_{\rm BKT}) = 1$ in the fits changes the estimate for $T_{\rm BKT}$ by up to 10–15% as shown in Fig. 8 for comparison.

VI. MAGNETOCALORICS AND THE T-B PHASE DIAGRAM

As we already discussed in Sec. III, the behavior of the magnetization $M(T)$ as a function of temperature plays an important role in determining the locations of the QPT. The interplay of magnetization with temperature is often termed magnetocalorics, which has been a fruitful field ever since the discovery of adiabatic demagnetization by Warburg in 1881 [38]. The central quantity of interest in this context is the cooling rate

$$\Gamma(B,T) = \frac{1}{T}\left(\frac{\partial T}{\partial B}\right)_S, \tag{21}$$

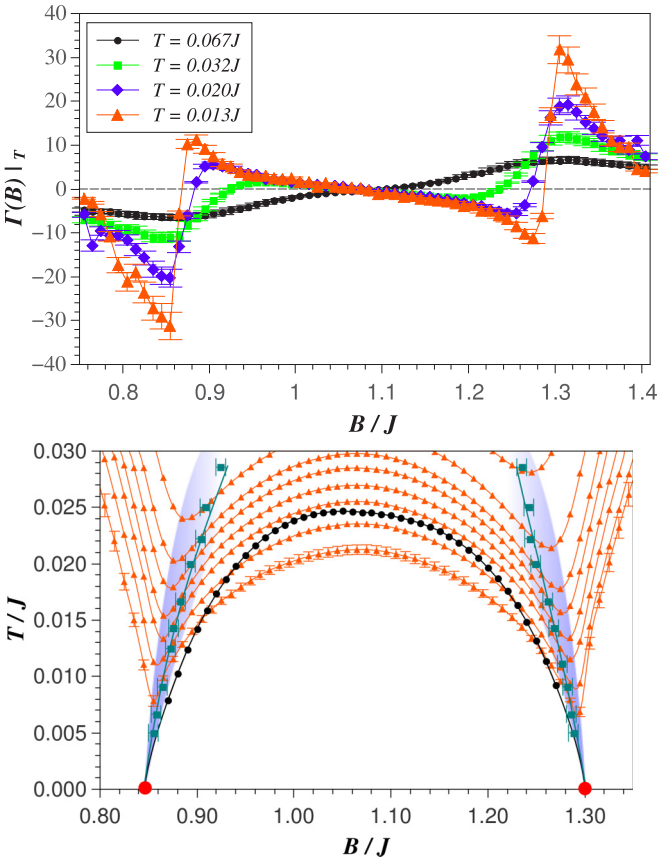

FIG. 9. (Color online) Top: QMC data for the cooling rate Γ as a function of field for different temperatures and $N = 676$. Bottom: Corresponding temperatures as a function of field for different values of constant entropy (red isentropes $dS = 0$) near B_c. The shaded region is dominated by large entropy, corresponding to the minima in the isentropes, which are relatively close to the maxima in the susceptibility (marked by green squares). The BKT transition T_{BKT} (connected dots) occurs at significantly lower temperatures.

which describes the temperature change with the applied field under adiabatic conditions. Using the cyclical rule and a Maxwell relation the cooling rate is also directly related to $M(T)$ and $S(B)$

$$\Gamma(B,T) = -\frac{1}{C}\left(\frac{\partial S}{\partial B}\right)_{\mathrm{T}} = -\frac{1}{C}\left(\frac{\partial M}{\partial T}\right)_{\mathrm{B}}, \qquad (22)$$

where $C = T(\frac{\partial S}{\partial T})_{\mathrm{B}}$ is the heat capacity. Therefore, the entropy is largest when $\Gamma = 0$.

The cooling rate for different temperatures is plotted in Fig. 9 (top), which shows sharp features near the QPT. In Ref. [39] it was predicted that the cooling rate diverges with a universal prefactor near the QPT, but we were not able to reach low enough temperatures to confirm this behavior.

Integrating the cooling rate in Eq. (21) gives the temperature as a function of field for a given entropy S. The corresponding isentropes are shown in Fig. 9 (bottom). The temperature reaches a minimum when the cooling rate is zero, which means that the entropy as a function of field (horizontal path) is maximal. It is interesting to notice that the points of maximum entropy $\Gamma = 0$ are relatively close to the maxima of the susceptibility. However, the maximum entropy region is *not* exactly at the value of the critical field as is the case for other systems without an ordered phase, as in the Ising chain [39]. Nor are those points associated with the finite-temperature BKT phase transition as would be the case for ordered systems in $D > 2$ [39]. The situation in $D = 2$ is therefore special, since in this case the sign change in the cooling rate $\Gamma = 0$ signals a maximum in the entropy in the crossover region where quantum critical behavior competes with vortex excitations in the shaded parameter range in Fig. 9 (bottom). The strong deviations between the maxima of entropy and susceptibility and the transition temperatures T_{BKT} occur at temperatures where the finite-temperature correlation length is smaller than the system size in our simulations, so that finite-size corrections are negligible in Fig. 9 (bottom).

VII. CONCLUSIONS

In summary, the magnetocaloric quantity $\partial M/\partial T$ turns out to be a universal indicator of the quantum critical behavior. We plot this quantity in Fig. 10 in the relevant T-B parameter space. On the one hand we have seen in Sec. III that the critical scaling is defined by a linear behavior of $M(T) \propto T$, which leads to a constant and large derivative $\partial M/\partial T$. The regions with quantum critical behavior therefore show up clearly in Fig. 10 as the lightest and darkest regions in the phase diagram above B_c and B_s, respectively. The points of $\Gamma \propto \partial M/\partial T = 0$ mark the boundaries towards regions, which are dominated by BKT vortex excitations. These points coincide with the maxima in the susceptibility, but are *not* directly associated with the QPT or the finite-temperature BKT phase transition. The BKT phase transition occurs at significantly lower temperatures and is not reflected by any directly measurable thermodynamic quantity [3]. Nonetheless, the predicted and well-established behavior of the spin stiffness at the BKT transition holds also for the dimer system, but strong corrections start to appear at small magnetization (i.e., boson density) as discussed in Sec. V.

We would like to emphasize that magnetocaloric measurements of $\partial M/\partial T$ not only allow a detailed analysis of the QPT, but also are potentially a very useful experimental tool

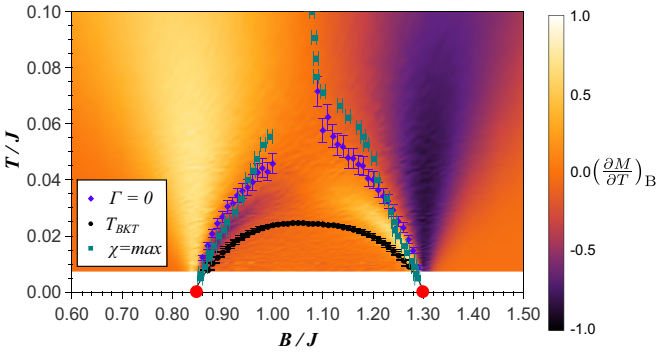

FIG. 10. (Color online) QMC data for the magnetocaloric derivative $\partial M/\partial T$ in the T-B parameter space for $N = 676$. The BKT transitions T_{BKT} is marked by connected dots (black), points of maximum entropy $\Gamma = 0$ by diamonds (violet), and maxima in the susceptibility by squares (green).

for identifying the effective dimensionality of the underlying spin systems due to the different density of states. In particular, for quasi-one-dimensional systems $\partial M/\partial T \propto 1/\sqrt{T}$ shows a characteristic divergence above the QPT, while for $D = 3$ we find an increase $\partial M/\partial T \propto \sqrt{T}$ analogous to the famous $T^{3/2}$ Bloch law. We find in our numerical simulations that $D = 2$ is characterized by perfectly linear behavior above the QPT, i.e., $\partial M/\partial T =$ constant without any detectable logarithmic corrections in contrast to the field theory prediction [16] in Eq. (12). As discussed in Sec. III this can be used to determine the exact positions of the critical field, which in turn allows the quantitative estimate of higher order terms in the analytical expressions as a function of the antiferromagnetic coupling constants.

ACKNOWLEDGMENTS

We are thankful for useful discussions with Raoul Dillenschneider, Achim Rosch, Markus Garst, Denis Morath, and Axel Pelster. This work was supported by the SFB Transregio 49 of the Deutsche Forschungsgemeinschaft (DFG) and the Allianz für Hochleistungsrechnen Rheinland-Pfalz (AHRP).

[1] A. Vogler, R. Labouvie, G. Barontini, S. Eggert, V. Guarrera, and H. Ott, Phys. Rev. Lett. **113**, 215301 (2014).
[2] Z. Hadzibabic *et al.*, Nature **441**, 1118 (2006).
[3] U. Tutsch *et al.*, Nat. Comm. **5**, 5169 (2014).
[4] S. Sachdev, Science **288**, 475 (2000).
[5] C. Ruegg *et al.*, Nature **423**, 62 (2003).
[6] S. Wessel, M. Olshanii, and S. Haas, Phys. Rev. Lett. **87**, 206407 (2001).
[7] K. Amaya, Y. Tokunaga, R. Yamada, Y. Ajiro, and T. Haseda, Phys. Lett. A **28**, 732 (1969).
[8] M. Tachiki and T. Yamada, J, Phys. Soc. Jpn. **28**, 1413 (1970).
[9] V. Berezinsky, Sov. Phys. JETP **32**, 493 (1971).
[10] V. Berezinsky, Sov. Phys. JETP **34**, 610 (1972).
[11] J. M. Kosterlitz and D. J. Thouless, J. Phys. C: Solid State Phys. **6**, 1181 (1973).
[12] J. M. Kosterlitz, J. Phys. C: Solid State Phys. **7**, 1046 (1974).
[13] K. Bernardet, G. G. Batrouni, J.-L. Meunier, G. Schmid, M. Troyer, and A. Dorneich, Phys. Rev. B **65**, 104519 (2002).
[14] O. Derzhko, J. Richter, O. Krupnitska, and T. Krokhmalskii, Phys. Rev. B **88**, 094426 (2013).
[15] S. Sachdev, *Quantum Phase Transitions* (Cambridge University, New York, 2011).
[16] S. Sachdev, T. Senthil, and R. Shankar, Phys. Rev. B **50**, 258 (1994).
[17] V. N. Popov, *Functional Integrals in Quantum Field Theory and Statistical Physics* (D. Reidel, Dordrecht, 1983).
[18] D. S. Fisher and P. C. Hohenberg, Phys. Rev. B **37**, 4936 (1988).
[19] S. Sachdev and E. R. Dunkel, Phys. Rev. B **73**, 085116 (2006).
[20] N. Prokof'ev and B. Svistunov, Phys. Rev. A **66**, 043608 (2002).
[21] N. Prokof'ev, O. Ruebenacker, and B. Svistunov, Phys. Rev. Lett. **87**, 270402 (2001).
[22] S. Sachdev and E. Demler, Phys. Rev. B **69**, 144504 (2004).
[23] S. Sachdev, Phys. Rev. B **59**, 14054 (1999).
[24] A. B. Harris, Phys. Rev. B **7**, 3166 (1973).
[25] T. Barnes, J. Riera, and D. A. Tennant, Phys. Rev. B **59**, 11384 (1999).
[26] M. Reigrotzki, H. Tsunetsugu, and T. M. Rice, J. Phys.: Condens. Matter **6**, 9235 (1994).
[27] O. F. Syljuåsen and A. W. Sandvik, Phys. Rev. E **66**, 046701 (2002).
[28] M. Matsumoto and T. Nishimura, ACM Trans. Model. Comput. Simul. **8**, 3 (1998).
[29] E. L. Pollock and D. M. Ceperley, Phys. Rev. B **36**, 8343 (1987).
[30] A. W. Sandvik, Phys. Rev. B **56**, 11678 (1997).
[31] M. E. Fisher, M. N. Barber, and D. Jasnow, Phys. Rev. A **8**, 1111 (1973).
[32] N. V. Prokof'ev and B. V. Svistunov, Phys. Rev. B **61**, 11282 (2000).
[33] R. G. Melko, A. W. Sandvik, and D. J. Scalapino, Phys. Rev. B **69**, 014509 (2004).
[34] H. Weber and P. Minnhagen, Phys. Rev. B **37**, 5986 (1988).
[35] K. Harada and N. Kawashima, J. Phys. Soc. Jpn. **67**, 2768 (1998).
[36] A. Cuccoli, T. Roscilde, V. Tognetti, R. Vaia, and P. Verrucchi, Phys. Rev. B **67**, 104414 (2003).
[37] Y.-D. Hsieh, Y.-J. Kao, and A. W. Sandvik, J. Stat. Mech.: Theory Exp. (2013) P09001.
[38] E. Warburg, J. Phys. Theor. Appl. **10**, 495 (1881).
[39] M. Garst and A. Rosch, Phys. Rev. B **72**, 205129 (2005).